Journal of Luminescence 203 (2018) 683–688

Contents lists available at ScienceDirect

Journal of Luminescence

journal homepage: www.elsevier.com/locate/jlumin

Understanding the mechanoluminescent mechanisms of manganese doped zinc sulfide based on load effects

Hui Zhou[a,b], Yide Du[a,b], Chen Wu[a,b], Yanjiao Jiang[b,c], Fu Wang[b], Jiachi Zhang[a,*], Zhaofeng Wang[b,*]

[a] National & Local Joint Engineering Laboratory for Optical Conversion Materials and Technology, Lanzhou University, Lanzhou, Gansu 730000, China
[b] State Key Laboratory of Solid Lubrication, Lanzhou Institute of Chemical Physics, Chinese Academy of Sciences, Lanzhou, Gansu 730000, China
[c] School of Stomatology, Lanzhou University, Lanzhou, Gansu 730000, China

ARTICLE INFO

Keywords:
ZnS: Mn^{2+}
Mechanoluminescence
Load effects
Trap model

ABSTRACT

In this work, manganese doped zinc sulfide (ZnS: Mn^{2+}) powder was synthesized, which was further composited with epoxy resin. In addition to the bright photoluminescence (PL), two types of mechanoluminescence (ML), i.e., friction and compression induced luminescence, were observed in ZnS: Mn^{2+}/epoxy composites. To deeply understand the mechanoluminescent mechanisms of ZnS: Mn^{2+}, the performance differences between PL and ML were investigated. The results suggested that the piezoelectric effect induced electroluminescence should not be the exact mechanism of ML. Moreover, load effects on the friction and compression induced ML as well as the thermoluminescence (ThL) were investigated. The variations of trap depth and carrier density in ZnS: Mn^{2+} before and after mechanics stimulation provided direct evidence that the release of electrons from traps should be responsible for ML. The load effects of ML also supported the proposed trap-based mechanisms, and the underlying theory was discussed in detail. This work first presents solid evidences for the trap-based mechanoluminescent mechanisms of ZnS: Mn^{2+} in elastic region.

1. Introduction

Mechanoluminescence (ML) is a phenomenon that materials emit light when they are mechanically stimulated, such as stretch, compression, impact, fracture, etc. [1–3]. Due to the widespread existence of mechanical activities in various fields, ML materials present great application values in lighting and displaying systems, mechanical sensors, aerospace and military damage detection, ceramic material crack monitoring and so on [2–8].

ML was first discovered by Sir Francis Bacon in 1605 when breaking the sugar crystals, which was called triboluminescence [8]. Till now, nearly 30% of organic molecular solids and 50% of inorganic compounds have been confirmed to have ML [2,9]. In the initial stage of ML research, it relied on the subjective visual observation of the ML response as a function of quantity and time [2]. In addition to the sucrose, researchers found ML from rocks, quartz, alkaline halide, molecular crystals, and some organic materials [8]. However, the discovered mechanoluminescent materials showed either low luminous efficiency or structural destruction. As a result, mechanoluminescent materials were initially thought to have no practical applications. In the year of 1999, C.-N. Xu and coworkers introduced strontium aluminate based mechanoluminescent materials into epoxy resin and obtained an mechanoluminescent elastic composite [7,10,11]. Such breakthrough generated ML with structural non-destruction, and opened the door for ML applications. Based on the above development, a series of decent work related to the applications of mechanoluminescent elastic composites have been explored, e.g., flexible handwriting device [12], mechanically driven light generator [13], non-contacting torque sensor [14], etc.

At present, rare earth doped strontium aluminate and transition metal doped zinc sulfide are well recognized as the representative mechanoluminescent materials for fabricating elastic composites [6,8,10,15–29], among which manganese doped zinc sulfide (ZnS: Mn^{2+}) has been proved to possess the highest mechanoluminescent efficiency (using PL quantum yield as a measurement of the efficiency of different mechanoluminescent materials) [2]. Although the mechanoluminescent elastic composites have attracted extensive attention recently, the basic physical theories still lack of research. Since mechanoluminescent materials are triggered by the mechanical stimulators, the relationship between the mechanics and mechanoluminescent properties should be comprehensively studied, which could not only allow deeply understanding the mechanoluminescent mechanisms, but

* Corresponding authors.
E-mail addresses: zhangjch@lzu.edu.cn (J. Zhang), zhfwang@licp.cas.cn (Z. Wang).

https://doi.org/10.1016/j.jlumin.2018.07.018
Received 7 November 2017; Received in revised form 31 May 2018; Accepted 18 July 2018
Available online 19 July 2018

also could guide the structural design of the composites for various applications.

In this work, ZnS: Mn^{2+} mechanoluminescent powders were synthesized and composited with epoxy resin. Two types of ML, i.e., friction and compression induced luminescence, were realized in the as-prepared composites. The doping concentration of Mn^{2+} was first optimized to obtain ZnS: Mn^{2+}/epoxy composites with the highest mechanoluminescent intensity. After that, the load effects on the friction and compression induced ML as well as the thermoluminescence (ThL) were investigated and discussed. Based on the load effects and the different behaviors between PL and ML, the underlying mechanisms for the ML of ZnS: Mn^{2+} in elastic region were demonstrated in detail.

2. Experimental

2.1. Materials and synthesis

ZnS: Mn^{2+} powders were synthesized by a solid state method. ZnS (≥ 99.99%), $MnCl_2{\cdot}4H_2O$ (≥ 99.0%), $MgCl_2{\cdot}6H_2O$ (≥ 98.0%) and NaCl (≥ 99.5%) were used without any further purification. $MgCl_2$ and NaCl were used as fluxing agents in this experiment, which accounted for 15 wt% of the raw materials with the molar ratio of $MgCl_2$ and NaCl to be 2: 3. The stoichiometric starting materials were mixed fully by grinding in an agate mortar. The mixture was then loaded into a corundum crucible and transferred to a muffle furnace (GSL-1600X). Then the mixture was sintered at 900 °C for 1 h under the atmosphere of nitrogen. After cooled to room temperature, the sample was taken out and washed by deionized water for three times to remove chlorides. The sample was dried in an oven and ZnS: Mn^{2+} powders were obtained. For synthesis of ZnS: Mn^{2+}/epoxy composites, 1.2 g of ZnS: Mn^{2+} powders were thoroughly mixed with 8.4 g of epoxy resin. The mixture was then transferred to a mold (4 cm in diameter and 0.8 cm in thickness) and cured at 60 °C for 3 h in an oven. Finally, ZnS: Mn^{2+}/epoxy composites were obtained.

2.2. Measurements and characterization

A Rigaku D/Max-2400 X-ray diffractometer (XRD) with Ni-filtered Cu Kα radiation (1.54056 Å) operating at 30 kV and 15 mA was used to check the crystalline phases of the obtained samples. The absorption spectra were measured on an ultraviolet-visible (UV–vis) spectrophotometer (PE lamda 950) using $BaSO_4$ as a reference. Photoluminescence (PL) emission and PL excitation spectra were recorded using a fluorescence spectrometer (Omni-λ300i) with a Xe 900 lamp (500 W) as the excitation source at room temperature. For PL tests, the slit width and scanning step were set to be 1.5 mm and 1 nm, respectively. The thermoluminescence (ThL) curves were detected using a FJ-417A ThL meter in the temperature range from 40 to 400 °C with a heating rate of 1 K s^{-1}. The frictional experiments were operated on a rotary friction testing machine (MS-T3001) by employing a self-made stainless steel friction pair with a radius of 0.2 mm under the rotational speed of 200 rpm. The compressive experiments were operated on a universal testing machine (WDT-5), which was preloaded to 200 N at a rate of 50 N/s and then loaded to 2000 N at a rate of 200 N/s. The produced ML of the ZnS: Mn^{2+}/epoxy composites was in situ detected by a spectrometer (Omni-λ300i) equipped with a CCD camera (IVAC-316) at a frame rate of 50 fps.

3. Results and discussion

The XRD patterns of the as-prepared ZnS: Mn^{2+} powders are shown in Fig. 1. It can be found that the variation of Mn^{2+} concentration shows no effect on the crystal phase. All diffraction peaks of the samples match well with those of the cubic sphalerite structure of ZnS (PDF#05–0566) without producing any impurity phase. The formation of cubic sphalerite structure of ZnS: Mn^{2+} should be attributed to the

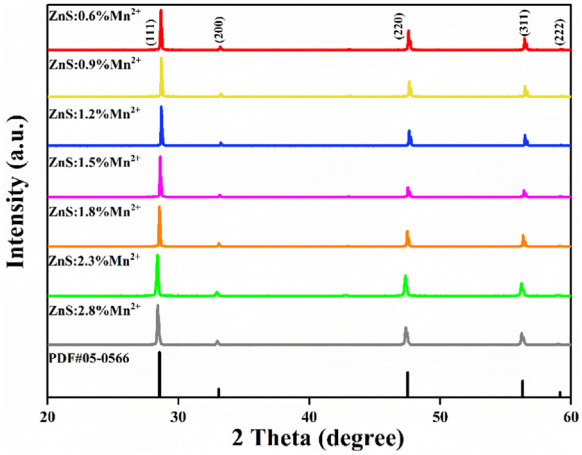

Fig. 1. XRD patterns of ZnS: Mn^{2+} powders with Mn^{2+} doping concentration from 0.6% to 2.8%.

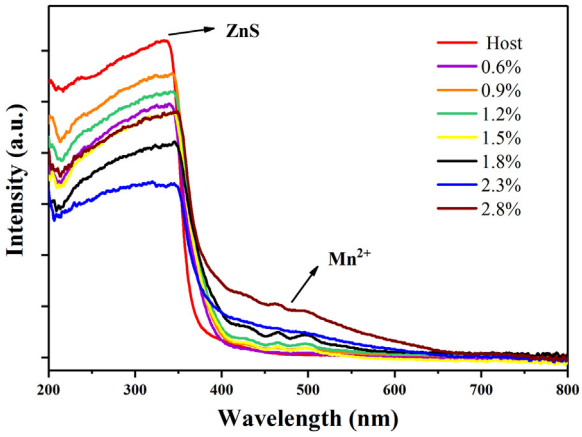

Fig. 2. UV–vis absorption spectra of ZnS and ZnS: Mn^{2+} measured at room temperature.

sintering temperature of 900 °C, which is lower than the transition temperature (1020 °C) from cubic to hexagonal phase in ZnS [30].

Fig. 2 shows the UV–vis absorption spectra of ZnS host and ZnS: Mn^{2+} samples. For ZnS host, the dominant absorption in the short-wave part (less than 340 nm) should be attributed to the fundamental band-to-band absorption [31]. For ZnS: Mn^{2+} powders, absorption band from 400 to 650 nm appeared compared with the host, which could be ascribed to the electron transfer between Mn^{2+} energy levels. When the doping concentration of Mn^{2+} was increased from 0.6% to 2.8%, the absorption band of Mn^{2+} enhanced monotonically. Such results suggest that Mn^{2+} ions have been successfully introduced in ZnS.

When irradiated by a UV light, ZnS: Mn^{2+} shows bright orange emissions. Fig. 3a shows the PL emission spectra of ZnS: Mn^{2+} samples under the excitation of 355 nm. Two broad bands, one from 400 to 530 nm and the other one from 530 to 700 nm, were found. They correspond to the zinc vacancy (V_{Zn}) emission and the $^4T_1 \rightarrow {}^6A_1$ electron transition of Mn^{2+}, respectively [32]. With the increase of the doping concentration, the $^4T_1 \rightarrow {}^6A_1$ emissions increase first and then decrease with the optimal Mn^{2+} doping concentration of 1.8%. Such concentration quenching is aroused by the competition between the radiative and non-radiative transitions of the luminescent centers [33]. It is also found that the emission intensity of V_{Zn} continuously decreases along with the increase of Mn^{2+} doping concentration. This is because that more Mn^{2+} doping would be beneficial to transfer the excitation energy to Mn^{2+} luminescence centers, and thus reduce the electron transfer rate to V_{Zn}. The PL excitation spectra of ZnS: Mn^{2+} monitored

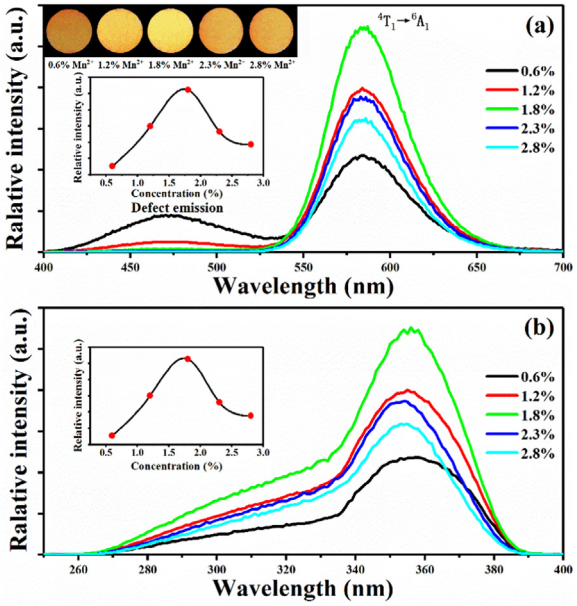

Fig. 3. (a) PL emission spectra (λ_{ex} = 355 nm) and (b) PL excitation spectra (λ_{em} = 585 nm) of the ZnS: Mn^{2+} samples; the insets in (a) are the corresponding PL emission photos and the PL emission intensity variation dependent on the doping concentration of Mn^{2+}; the inset in (b) shows the PL excitation intensity variation dependent on the doping concentration of Mn^{2+}.

by 585 nm are presented in Fig. 3b, which shows similar intensity variation trend with the $^4T_1 \rightarrow {}^6A_1$ emission in PL.

ZnS: Mn^{2+} is a well-known mechanoluminescent materials because of its high luminescent efficiency. To obtain elastic ML, ZnS: Mn^{2+} powders were further composite with epoxy resin. When the surface of ZnS: Mn^{2+}/epoxy composites was scratched or rubbed, intense luminescence could be emitted, which was bright enough to be catched by naked eyes as shown in the inset of Fig. 4. Such behavior is called friction induced luminescence or triboluminescence, which is one type of ML. The friction induced mechanoluminescent spectra of ZnS: Mn^{2+}/epoxy composites are shown in Fig. 4, in which there is only one broad emission band corresponding to the $^4T_1 \rightarrow {}^6A_1$ electron transition of Mn^{2+}. It should be noted that the emission of V_{Zn} in ZnS: Mn^{2+} in blue-green light region is absent in the mechanoluminescent spectra. In addition, the optimal doping concentration for ML is 0.9%, which is far below that of the PL doping concentration (1.8%). Both of the absence of the V_{Zn} emission and the different optimal doping concentration

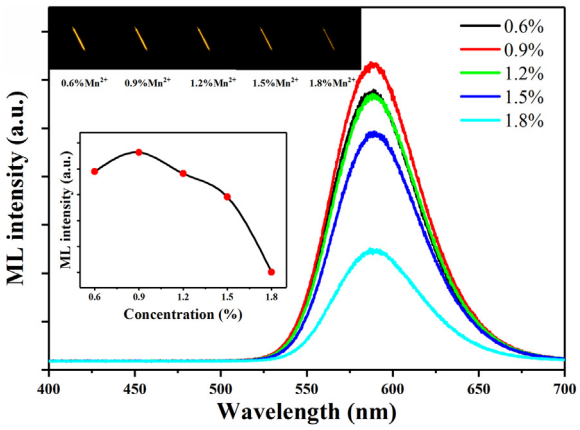

Fig. 4. The friction induced mechanoluminescent spectra of ZnS: Mn^{2+}/epoxy composites with Mn^{2+} doping concentration from 0.6% to 1.8%; the insets show the corresponding mechanoluminescent photos and the mechanoluminescent intensity variation as a function of doping concentration.

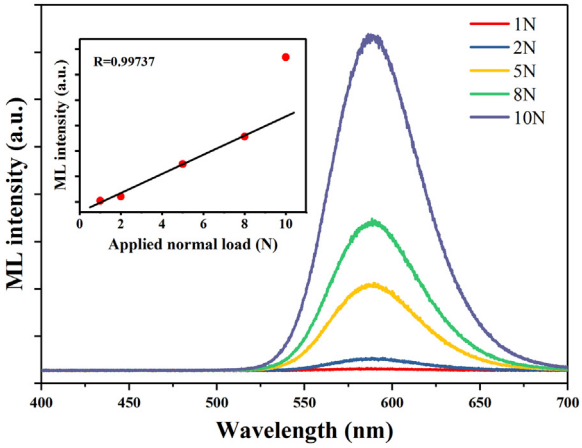

Fig. 5. The friction induced ML spectra of ZnS: Mn^{2+}/epoxy composites with the Mn^{2+} doping concentration of 0.9% under different normal loads; the inset is the relationship between mechanoluminescent intensity and the applied normal load for the friction induced ML.

suggest that the mechanoluminescent mechanism should be different from that of PL. Previous reports proposed that the possible mechanoluminescent mechanisms of ZnS: Mn^{2+} should come from the piezoelectric effect induced electroluminescence [34]. However, it is found that the electroluminescent spectra of ZnS: Mn^{2+} in literatures also showed obvious emission of V_{Zn} [35]. It indicates that the piezoelectric effect induced electroluminescence should not be the exact mechanism of ML.

Since ML is the process stimulated by mechanics, it is highly important to directly establish the relationship between the mechanical behaviors and mechanoluminescent properties to explore the underlying mechanoluminescent mechanisms. Fig. 5 shows the friction induced mechanoluminescent spectra of ZnS: Mn^{2+}/epoxy composites under various applied normal loads. The mechanoluminescent spectra were tested in situ on a friction testing machine (MS-T3001) by employing a stainless steel tip as the upper friction pair, and the rotation speed and radius were kept constant. Along with the increase of the normal load from 1 to 10 N, the friction induced mechanoluminescent intensity was gradually increased (as shown in the inset of Fig. 5). It should be noted that the variation of mechanoluminescent intensity is almost linear when the applied load is below 8 N. However, the increase of the mechanoluminescent intensity exceeds the linear variation region when the applied normal load is higher than 8 N. This is because that too high normal load could cause remarkable surface destruction of the elastic composites. The determined ML at the applied load of 10 N is actually the integrated emission from both of the surface and interior of the composites, aroused by elastic and plastic deformation as well as fracture. Since this work focused on the ML of ZnS: Mn^{2+} in elastic region, the last data point in the inset of Fig. 5 was excluded for fitting.

In addition to the friction induced ML, the ZnS: Mn^{2+}/epoxy composites could also show ML by compression. Fig. 6 exhibits the compression induced ML spectrum of ZnS: Mn^{2+}/epoxy composites with the doping concentration of Mn^{2+} at 0.9% under a load of 1000 N. The ML spectrum was tested in situ on a universal testing machine (WDT-5) at a loading speed of 200 N/s from 200 to 2000 N. The compression induced ML spectrum shows same shape and peak location as those of friction induced luminescence. The overall variation of the compression induced mechanoluminescent intensity is similar to the ML induced by friction that it gradually increases with increasing the applied compression load. The mechanoluminescent intensity increases linearly first when the applied load is below 1300 N. However, when the compression load is further increased from 1300 to 2000 N, the variation degree of mechanoluminescent intensity is decreased, which is different from that of the friction induced ML.

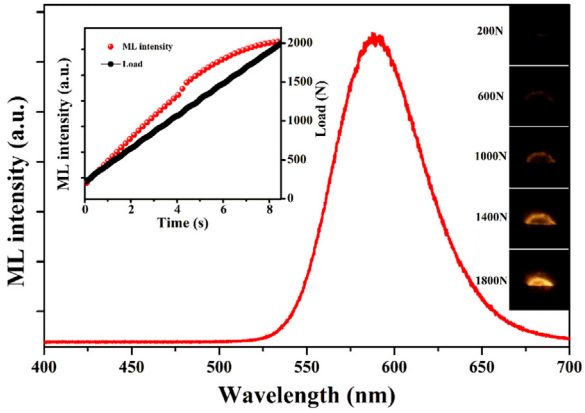

Fig. 6. Compression induced ML spectrum of ZnS: Mn^{2+}/epoxy composites with the Mn^{2+} doping concentration of 0.9% under load of 1000 N; the upper left inset shows the variations of emission intensity and applied load as a function of time for the compression induced ML; the right insets show the mechanoluminescent photos of the ZnS: Mn^{2+}/epoxy composites under various applied loads.

To further explore the reasons of the above mechanoluminescent behaviors as a function of load, ThL spectra of the ZnS: Mn^{2+} before and after compression was measured as shown in Fig. 7. The position of ThL band represents the trap depth, whereas lower temperature represents to shallow traps and higher temperatures corresponds to deeper traps. The exact trap type, trap depth and carrier density could be calculated by a classical multi-peak fitting method developed by Chen et al. as shown in Eq. (1) [36].

$$I(T) = sn_0\exp\left(-\frac{E}{kT}\right)\left[1 + (b-1)\frac{s}{v}\times\int_{T_0}^{T}\exp\left(-\frac{E}{kT'}\right)dT'\right]^{-\frac{b}{b-1}} \quad (1)$$

where I is the glow-peak intensity, s is the frequency factor, and n_0 is the concentration of trapped carriers, E is the trap depth, k is the Boltzmann constant, b is the kinetics order parameter, and v is the heating rate (1 K s^{-1} for our experiment). According to the work by Kitis et al. [37], Eq. (1) could be simplified to Eq. (2), and the values of s and n_0 can be expressed by introducing the parameters I_m and T_m, where I_m represents the glow-peak maximum intensity and T_m is the temperature at the maximum.

$$I(T) = I_m b^{\frac{b}{b-1}}\exp\left(\frac{E}{kT}\frac{T-T_m}{T_m}\right) \times\left[(b-1)(1-\Delta)\frac{T^2}{T_m^2}\exp\left(\frac{E}{kT}\frac{T-T_m}{T_m}\right)+Z\right]^{-\frac{b}{b-1}} \quad (2)$$

$$s = \frac{vE}{KT_m{}^2}\frac{1}{Z}\exp\left(\frac{E}{kT_m}\right) \quad (3)$$

$$n_0 = \frac{kT_m{}^2}{vE}I_m Z\left(\frac{b}{Z}\right)^{\frac{b}{b-1}} \quad (4)$$

$$\Delta = \frac{2kT}{E},\ Z = 1 + (b-1)\frac{2kT_m}{E} \quad (5)$$

The calculated values of trap depth (E), kinetics order parameter (b), frequency factor (s) and carrier density (n_0) are summarized in Table 1. Two kinds of traps located at different depths were determined (Trap 1 and trap 2 correspond to the shallow and deep traps, respectively). Comparing the trap depths as well as the carrier densities before and after compression at an applied load of 1000 N, it is obviously found

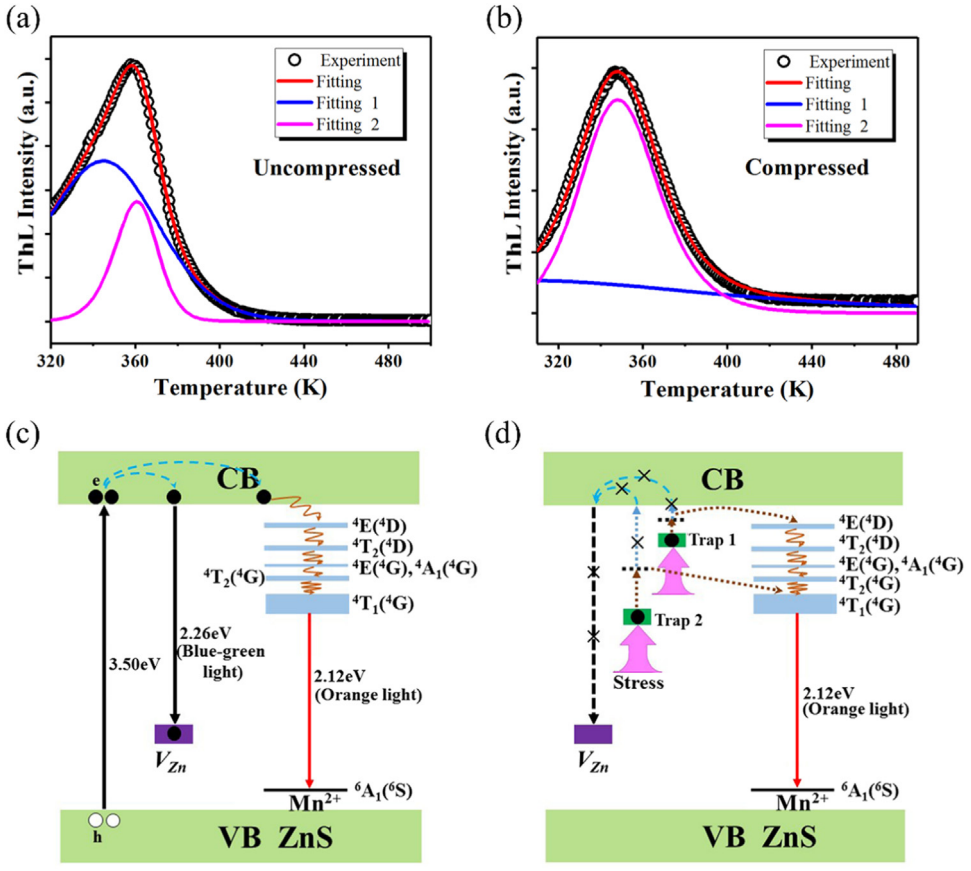

Fig. 7. ThL curves of ZnS: Mn^{2+} (a) before and (b) after compression under a load of 1000 N; diagrams for the processes of (c) PL and (d) ML.

Table 1
Fitting parameters of ThL peaks before and after compression at a load of 1000 N.

Samples	Fitting	E (eV)	b	s (s^{-1})	n_o (cm^{-3})
Uncompressed	1	0.419	1.385	4.444×10^4	2.927×10^5
	2	1.374	1.552	1.692×10^{18}	7.703×10^4
Compressed	1	0.111	2	4.458×10^{-1}	1.746×10^4
	2	0.759	1.889	5.923×10^5	1.863×10^4

that the trap depth moves to shallow position regardless trap 1 or trap 2. Moreover, most of the trapped carriers are released after compression. Since the applied compression corresponds to the mechanoluminescent process, the observation of released carries provides a direct evidence for the mechanism that the trapped carries should be responsible for ML. Therefore, a trap-based mechanoluminescent mechanism is proposed as shown in Fig. 7d. For the PL processes (Fig. 7c), electrons were first excited from valence band (VB) to conduction band (CB) by the UV light. Most of the excited electrons were transferred to the excited levels of Mn^{2+}, generating the characteristic orange emission band. The rest of the excited electrons were then transferred to the energy levels of V_{Zn}, producing the blue-green luminescence via the recombination of electrons and holes. For ML (Fig. 7d), the stored electrons in the traps could be released under a stress stimulation. Because there was no defect state (V_{Zn}) emission in the mechanoluminescent spectra of ZnS: Mn^{2+}, the exact migration processes of the released electrons should be directly from traps to the excited state levels of Mn^{2+} based on the tunneling effects. It should be noticed that the PL of ZnS: Mn^{2+} comes from the continuous excitation of the UV light, while the ML is originated from the energy of released electrons. With the increase of Mn^{2+} concentration, the energy transfer efficiency from the trapped electrons to Mn^{2+} would be increased first. However, since the amount of trapped electrons in ZnS: Mn^{2+} is limited, the energy transfer in ML is not as continuous as that in photoluminescent process. As a result, the ML of ZnS: Mn^{2+} shows a relatively low quenching concentration (Fig. 4).

In addition to explain the absent of defect state emission and low quenching concentration of ML, the trap-related mode could also be utilized to explain the relationships between load and mechanoluminescent intensity in both of friction and compression induced luminescence. Based on the theory developed by Chandra et al. [38], the total number of released electrons from traps can be expressed as:

$$n_t = aQ^2 \tag{6}$$

where a is a constant and Q is the surface charge density.

By differentiating Eq. (5), the release rate of the trapped electrons can be described as:

$$v = \frac{dn_t}{dt} = 2aQ\frac{dQ}{dt} \tag{7}$$

The pressure should theoretically reach the set value in a moment. However, in the actual experiment process, the pressure reaches the set value should take a certain time. Taking d_0 as the localized piezoelectric constant near the Mn^{2+} centers, P_0 as the set pressure, t as the time for the rise of pressure, and ζ as the rate-constant for the rise of pressure, the generation rate of piezoelectric charges can be expressed as:

$$v_q = d_o\frac{dP}{dt} = d_oP_o\zeta\exp(-\zeta t) \tag{8}$$

Since the surface charge density depends on the released electrons from traps and the relaxation of the electrons, the change rate of the surface charge density could be evolved to:

$$\frac{dQ}{dt} = v_q - \gamma Q = d_oP_o\zeta\exp(-\zeta t) - \gamma Q \tag{9}$$

where γ is the rate-constant for the relaxation of surface charges. By integrating Eq. (8) and taking $Q = 0$, at $t = 0$, the following equation is obtained:

$$Q = \frac{d_oP_o\zeta}{(\zeta-\gamma)}[\exp(-\gamma t) - \exp(-\zeta t)] \tag{10}$$

In this experiment, the deformation of the samples was fixed at a strain rate, which arouse the detrapping of the electrons. Therefore, dQ/dt should be constant (represented by c). Using Eqs. (7) and (10), the release rate of the trapped electrons is given by:

$$v = \frac{dn_t}{dt} = 2aQ\frac{dQ}{dt} = 2ac\frac{d_oP_o\zeta}{(\zeta-\gamma)}[\exp(-\gamma t) - \exp(-\zeta t)] \tag{11}$$

Since the pressure reaches the set pressure at a fast speed (ζ is much larger than γ), the release rate of electrons v is approximately equal to the electron-hole recombination rate R:

$$R \approx v = 2ac\frac{d_oP_o\zeta}{(\zeta-\gamma)}[\exp(-\gamma t) - \exp(-\zeta t)] \tag{12}$$

Therefore, the mechanoluminescent intensity at a certain time can be expressed as:

$$I = \eta R = 2\eta ac\frac{d_oP_o\zeta}{(\zeta-\gamma)}[\exp(-\gamma t) - \exp(-\zeta t)] \tag{13}$$

where η is the emitting efficiency of Mn^{2+} centers during electron-hole recombination.

By differentiating Eq. (13) and equating it to 0, the time t_0 corresponding to the strongest emission of ML can be expressed as:

$$t_0 = \frac{1}{\zeta-\gamma}\ln\frac{\zeta}{\gamma} \tag{14}$$

By substituting the value of t_0 from Eq. (14) in Eq. (13), the strongest intensity of ML could be obtained. Because ζ is much larger than γ, the strongest intensity of ML I_0 is approximately given by:

$$I_0 = 2\eta ac\frac{d_oP_o\zeta}{(\zeta-\gamma)} \times \left[\frac{(\zeta-\gamma)}{\gamma} \times \left(\frac{\gamma}{\zeta}\right)^{1/\left(1-\frac{\gamma}{\zeta}\right)}\right] \approx 2\eta acd_oP_o \tag{15}$$

Since a, c, η and d_0 are fixed values, it is obvious that the strongest mechanoluminescent intensity should be linear with set load in a suitable range, which is consistent with the observations in both friction and compression induced ML. Similar to the explanation of the lowered quenching concentration, the amount of trapped electrons in ZnS: Mn^{2+} is limited. Therefore, the linear relationship between load value and mechanoluminescent intensity should appear under a suitable mechanical stimulation with sufficiently releasing the electrons. When the compression load is higher than 1300 N, the amount of released electrons from traps is insufficient to maintain the theoretic linear relationship. As a result, the intensity variation as a function of load (higher than 1300 N) of compression induced ML is slowed down as observed in Fig. 6.

4. Conclusions

In Summary, ZnS: Mn^{2+} and ZnS: Mn^{2+}/epoxy composites were synthesized in this work. By comparing the PL and ML, it is found that the ML of ZnS: Mn^{2+} shows no emission from the defect of V_{Zn}, while its quenching concentration is far below that of PL. Such performance differences suggest that the mechanism of ML should be different from that of PL. The load effect on the ThL properties of ZnS: Mn^{2+} presents direct evidence that the migration of electrons from traps should be responsible for ML, which could well explain the above different spectral behaviors between PL and ML. The investigation of the relationship between mechanoluminescent intensity and loads in both friction and compression induced luminescence further confirms the proposed trap model, and the underlying theory is discussed in detail.

This work presents solid evidences for the mechanoluminescent mechanisms of ZnS: Mn^{2+} in elastic region, which is valuable for the structural design of mechanoluminescent materials for various applications.

Acknowledgments

This work is supported by the CAS Pioneer Hundred Talents Program, and the Natural Science Foundation of Gansu Province (17JR5RA319).

References

[1] J. Verhoeven, Pure Appl. Chem. 68 (1996) 2223–2286.
[2] D.O. Olawale, T. Dickens, W.G. Sullivan, O.I. Okoli, J.O. Sobanjo, B. Wang, J. Lumin. 131 (2011) 1407–1418.
[3] D.O. Olawale, K. Kliewer, A. Okoye, T.J. Dickens, M.J. Uddin, O.I. Okoli, J. Lumin. 147 (2014) 235–241.
[4] G.J. Yun, M.R. Rahimi, A.H. Gandomi, G.-C. Lim, J.-S. Choi, Smart Mater. Struct. 22 (2013) 055006.
[5] B. Chandra, Int. J. Lumin. Appl. 2 (2012) 44–72.
[6] K.-S. Sohn, M.Y. Cho, M. Kim, J.S. Kim, Opt. Express 23 (2015) 6073–6082.
[7] C. Xu, T. Watanabe, M. Akiyama, X. Zheng, Mater. Res. Bull. 34 (1999) 1491–1500.
[8] S.M. Jeong, S. Song, K.-I. Joo, J. Kim, S.-H. Hwang, J. Jeong, H. Kim, Energy Environ. Sci. 7 (2014) 3338–3346.
[9] D. Peng, B. Chen, F. Wang, ChemPlusChem 80 (2015) 1209–1215.
[10] C.-N. Xu, T. Watanabe, M. Akiyama, X.-G. Zheng, Appl. Phys. Lett. 74 (1999) 2414–2416.
[11] C. Xu, T. Watanabe, M. Akiyama, X. Zheng, Appl. Phys. Lett. 74 (1999) 1236–1238.
[12] X. Wang, H. Zhang, R. Yu, L. Dong, D. Peng, A. Zhang, Y. Zhang, H. Liu, C. Pan, Z.L. Wang, Adv. Mater. 27 (2015) 2324–2331.
[13] S.M. Jeong, S. Song, S.-K. Lee, B. Choi, Appl. Phys. Lett. 102 (2013) 051110.
[14] J.S. Kim, G.-W. Kim, Sens. Actuators A: Phys. 218 (2014) 125–131.
[15] C.-N. Xu, H. Yamada, X. Wang, X.-G. Zheng, Appl. Phys. Lett. 84 (2004) 3040–3042.
[16] K.S. Sohn, S.Y. Seo, Y.N. Kwon, H.D. Park, J. Am. Ceram. Soc. 85 (2002) 712–714.
[17] J.S. Kim, K. Kibble, Y.N. Kwon, K.-S. Sohn, Opt. Lett. 34 (2009) 1915–1917.
[18] K.-S. Sohn, W.B. Park, S. Timilsina, J.S. Kim, Opt. Lett. 39 (2014) 1410–1413.
[19] J.S. Kim, Y.-N. Kwon, N. Shin, K.-S. Sohn, Acta Mater. 53 (2005) 4337–4343.
[20] S. Timilsina, K.H. Lee, I.Y. Jang, J.S. Kim, Acta Mater. 61 (2013) 7197–7206.
[21] S. Timilsina, K.H. Lee, Y.N. Kwon, J.S. Kim, J. Am. Ceram. Soc. 98 (2015) 2197–2204.
[22] Y. Chen, J. Duh, B. Chiou, C. Peng, Thin Solid Films 392 (2001) 50–55.
[23] A.A. Bol, J. Ferwerda, J.A. Bergwerff, A. Meijerink, J. Lumin. 99 (2002) 325–334.
[24] L. Qi, B.I. Lee, J.M. Kim, J.E. Jang, J.Y. Choe, J. Lumin. 104 (2003) 261–266.
[25] A. Ishizumi, C. White, Y. Kanemitsu, Appl. Phys. Lett. 84 (2004) 2397–2399.
[26] W. Peng, G. Cong, S. Qu, Z. Wang, Opt. Mater. 29 (2006) 313–317.
[27] Y.-T. Nien, I.-G. Chen, ECS Trans. 19 (2009) 1–6.
[28] S. Leelachao, S. Muraishi, T. Sannomiya, J. Shi, Y. Nakamura, J. Lumin. 170 (2016) 24–29.
[29] M.-C. Wong, L. Chen, M.-K. Tsang, Y. Zhang, J. Hao, Adv. Mater. 27 (2015) 4488–4495.
[30] B. Fitzpatrick, J. Cryst. Growth 86 (1988) 106–110.
[31] K. Sooklal, B.S. Cullum, S.M. Angel, C.J. Murphy, J. Phys. Chem. 100 (1996) 4551–4555.
[32] S. Akanksha, L. Mukta, S. Shashi, L. Niranjan Prasad, M. Chantal Khan, K. Sulabha, Nanotechnology 19 (2008) 245613.
[33] Z. Wang, Y. Li, Q. Jiang, H. Zeng, Z. Ci, L. Sun, J. Mater. Chem. C 2 (2014) 4495–4501.
[34] H. Matsui, C.-N. Xu, Y. Liu, H. Tateyama, Phys. Rev. B 69 (2004) 235109.
[35] H. Yang, P.H. Holloway, B.B. Ratna, J. Appl. Phys. 93 (2003) 586–592.
[36] R. Chen, J. Electrochem. Soc. 116 (1969) 1254–1257.
[37] G. Kitis, J.M. Gomez-Ros, J.W.N. Tuyn, J. Phys. D: Appl. Phys. 31 (1998) 2636.
[38] B. Chandra, C. Xu, H. Yamada, X. Zheng, J. Lumin. 130 (2010) 442–450.